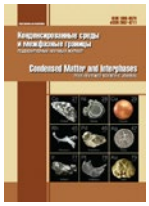

ISSN 1606-867X (Print)
ISSN 2687-0711 (Online)
Condensed Matter and Interphases
Kondensirovannye Sredy i Mezhfaznye Granitsy
https://journals.vsu.ru/kcmf/

Review

Review article
https://doi.org/10.17308/kcmf.2026.28/13410

Crystal growth and optical properties of SrB_4O_7: a review

T. N. Khamaganova✉, **A. K. Subanakov**

Baikal Institute of Nature Management Siberian branch of the Russian Academy of Sciences, 6, Sakhyanovoy st., Ulan-Ude 670047, Buryatia, Russian Federation

Abstract

Objective: This review systematically summarizes the available literature on crystal growth methods and conditions, polymorphism, crystal structures, and optical properties of strontium tetraborate (SrB_4O_7) (SBO). Large bulk single crystals have been successfully grown using several techniques, including the Czochralski, Kyropoulos, micro-pulling-down (μ–PD), and top-seeded solution growth (TSSG) methods. The advantages and limitations of each approach are discussed, along with the challenges encountered during growth and strategies for their resolution. SBO crystallizes in two polymorphic modifications: a stable high-temperature α-form (orthorhombic, space group $Pmn2_1$) and a metastable low-temperature β-form (trigonal, space group $P3$). During crystal growth, α-SBO single crystals tend to form irregular domain structures that give rise to quasi-phase matching (QPM), which is essential for efficient nonlinear optical frequency conversion.

Conclusions: The results of investigations into the thermal, mechanical, elastic, piezo-optical, acousto-optical, and nonlinear optical properties of SBO crystals are presented. Current developments in exploiting SBO domain structures for radiation generation across a broad spectral range are also discussed. In addition, the potential of SBO single crystals as paraelectric materials for ultra-compact microresonators is considered, particularly for wavelength conversion of coherent radiation in the deep- and vacuum-ultraviolet (VUV) regions.

Keywords: Strontium tetraborate, Polymorphism, SBO single crystals, Czochralski method, Crystal structures, Irregular domains, Wavelength conversion

Funding: This work was supported by the Ministry of Science and Higher Education of the Russian Federation (State Assignment to Baikal Institute of Nature Management SB RAS, No. 0273-2021-0008).

For citation: Khamaganova T. N., Subanakov A. K. Crystal growth and optical properties of SrB4O7: a review. *Condensed Matter and Interphases*. 2026;28(3): 333–349. https://doi.org/10.17308/kcmf.2026.28/13410

✉ Tatyana N. Khamaganova, e-mail: khama@binm.ru
© Khamaganova T. N., Subanakov A. K., 2026

The content is available under Creative Commons Attribution 4.0 License.

Обзор

Обзорная статья
УДК 546.07.273+535.32/58
Научная специальность ВАК – 1.4.15. Химия твердого тела
https://doi.org/10.17308/kcmf.2026.28/13410

Выращивание кристаллов и оптические свойства SrB_4O_7. Обзор

Т. Н. Хамаганова✉, А. К. Субанаков

ФГБУН Байкальский институт природопользования Сибирского отделения Российской академии наук, ул. Сахьяновой, 6, Улан-Удэ 670047, Республика Бурятия, Российская Федерация

Аннотация

Цель статьи: В обзоре обобщены и систематизированы литературные данные по методам и условиям выращивания кристаллов, полиморфизме, кристаллических структурах и оптических свойствах тетрабората стронция (SrB_4O_7). Показано, что крупные объемные монокристаллы могут быть получены несколькими методами, среди которых методы Чохральского, Киропулоса, микровытягивания вниз (μ–PD), из раствора с верхней затравкой (TSSG). Рассмотрены преимущества и недостатки представленных методов выращивания кристаллов, а также проблемы, возникающие в процессе роста и пути их устранения. SrB_4O_7 (SBO) кристаллизуется в двух полиморфных модификациях, одна из которых стабильная высокотемпературная α-форма (ромбическая ячейка, пр. гр. $Pmn2_1$), другая – метастабильная низкотемпературная β-форма (тригональная ячейка, пр. гр. $P\bar{3}$).

Монокристаллы α-SrB_4O_7 в процессе роста образуют нерегулярные домены, приводящие к квазифазовому синхронизму, необходимому для эффективного нелинейного оптического преобразования света.

Выводы: Представлены результаты исследований термических, механических, упругих, пьезооптических, акустооптических и нелинейно-оптических свойств кристаллов SBO. Обсуждены актуальные направления использования доменных структур SBO, обеспечивающих генерацию излучения в широком диапазоне спектра.

Рассмотрены перспективы применения монокристаллов SrB_4O_7 как параэлектрического материала в сверхкомпактных микрорезонаторных устройствах преобразования длины волны когерентного излучения в глубоком УФ- и ВУФ-диапазонах.

Ключевые слова: тетраборат стронция, полиморфизм, монокристаллы SrB_4O_7, метод Чохральского, кристаллические структуры, нерегулярные домены, преобразования длины волны

Источник финансирования: Работа выполнена при финансовой поддержке Министерства науки и высшего образования РФ (Государственное задание БИП СО РАН № 0273-2021-0008).

Для цитирования: Хамаганова Т. Н., Субанаков А. К. Выращивание кристаллов и оптические свойства SrB_4O_7. Обзор. *Конденсированные среды и межфазные границы*. 2026;28(3): 333–349. https://doi.org/10.17308/kcmf.2026.28/13410

✉ Хамаганова Татьяна Николаевна, e-mail: khama2025@bk.ru
© Хамаганова Т. Н., Субанаков А. К., 2026

1. Introduction

Single crystals of SBO combine outstanding physicochemical properties, chemical stability, high thermal conductivity, a high optical damage threshold, appreciable optical nonlinearity, and a wide transparency window, making them promising materials for piezoelectric, nonlinear optical, laser, and luminescent device applications [1–7].

Two polymorphic modifications of strontium tetraborate are known: the stable high-temperature orthorhombic α-form and the metastable low-temperature trigonal β-form. No consensus exists in the literature regarding the space group setting of orthorhombic SBO; three crystallographic settings of the same space group have been reported by different authors. The crystal structure of orthorhombic α-SBO has been investigated by numerous groups. The first structure determination was carried out by Krogh-Moe in the standard crystallographic setting of space group $Pmn2_1$ [8], a description that has also been adopted in [9–15]. Subsequently, alternative refinements were performed in space group $P2_1nm$ [3, 16, 17], while other studies have assigned the structure to $Pnm2_1$ [1, 2, 4–6, 18–22]. Although the work in [1] established the promise of SBO and stimulated extensive subsequent investigations, the non-standard space group setting adopted therein, and carried over by many later authors, is highly inconvenient. The resulting inconsistency in structural data created significant difficulties in interpreting and comparing results, particularly

with respect to crystal growth along specific crystallographic axes and the tensorial description of optical properties.

The structure of α-SBO consists of a rigid three-dimensional framework of corner-sharing BO_4 tetrahedra, with nine-coordinate strontium atoms occupying the interstitial voids. The metastable low-temperature β-SBO form crystallizes in the trigonal system, space group *P*3, with unit cell parameters *a* = 17.145(1) Å, and *c* = 4.2527(5) Å [23]. The non-centrosymmetric unit cell contains five Sr atoms (three in special positions), twelve B atoms, and twenty-one O atoms. Its structure comprises BO_3 triangles and BO_4 tetrahedra in a 1:1 ratio. Pairs of BO_3 triangles are connected to BO_4 tetrahedra through shared corners to form chains, which are in turn interconnected via common corners to generate a three-dimensional framework with channels running parallel to [001]. The Sr^{2+} ions reside within these channels and adopt strongly distorted coordination polyhedra with coordination numbers of 9, 10, and 12. The density of β-SBO is considerably lower than that of the α-modification, which is built exclusively from BO_4 tetrahedra. The crystal structure of β-SBO was determined by Vasiliev et al. [23] from a single crystal isolated during the crystallization of $SrO{\cdot}2B_2O_3$ glass. Both polymorphic modifications of SBO possess a unique combination of physical properties that makes them highly attractive for research.

In quantum electronics and laser technology, there is a pressing need for materials capable of generating coherent radiation in the VUV with broad spectral coverage. Against this background, nonlinear SBO crystals have attracted particular attention: they combine a wide transparency window extending to 125 nm [1] with large nonlinear coefficients and a high optical damage threshold [1, 2, 5]. Their small birefringence, however, and the consequent absence of angle phase-matching, limits their use in conventional nonlinear optical configurations [1]. Notwithstanding this limitation, SBO crystals may find application in autocorrelation measurements of femtosecond pulses via nonlinear optical conversion at λ = 125 nm [2]. An alternative route to efficient nonlinear optical conversion was QPM, which can be realized through irregular domain structures [24, 25].

The ability of α-SBO single crystals to form extended domains during growth [11, 19–22], together with reported values of their thermal conductivity and thermal expansion [26, 27] and their mechanical and strength properties [12], substantially broadens the range of potential applications.

The present review systematically surveyed the crystal growth methods and functional properties of SBO, compared its optical and mechanical characteristics with those of other mono- and divalent metal borates, and discussed prospective application areas on the basis of available literature data.

2. Crystal growth methods for SBO single crystals

Strontium tetraborate melts congruently at approximately 1000 °C. Although congruent melting was consistently reported in the literature, published values of the melting temperature varied among different authors, with only two studies reporting nearly identical values (Table 1). The β→α phase transition was investigated on optically homogeneous β-SBO single crystals using differential scanning calorimetry (DSC) [30]. The DSC curve exhibited an exothermic event in the range 820–870 °C corresponding to the irreversible transformation to the stable orthorhombic α-modification, followed by an endothermic event attributed to melting of this phase. The obtained data are consistent with the

Table 1. Thermal properties of SrB_4O_7

$T_{phase\ transition}$, °C (β→α)	$T_{melting\ point}$, °C	Melting character	Reference
	994±10	Congruent	[28]
	970	Congruent	[17]
	1015±5	Congruent	[29]
820–870	1000±2	Congruent	[30]
	1017	Congruent	[31]

results of [32], in which traces of a metastable phase were recorded at 850 °C.

Owing to the excellent physicochemical characteristics of SBO crystals [1–7], demand for large, fully transparent, high-quality material continues to grow. Because the choice of crystal growth method is governed by melting behavior, the congruent melting of SBO enabled direct growth from the melt by conventional techniques (the Czochralski [1, 2, 4, 10, 17, 18, 21, 25, 27, 33] and Kyropoulos [3, 34, 35] methods), as well as by their respective modifications: the μ–PD [15, 31, 36] and TSSG [5, 37].

2.1. Czochralski method

The Czochralski method was used in the majority of published studies on SBO single crystal growth. According to [1, 17], a mixture of high-purity $SrCO_3$ and H_3BO_3 was heated to approximately 100 °C above the melting point, and the platinum crucible containing the melt was placed in a resistance furnace such that the temperature gradient in the surface layer was 80–100 °C/cm. Complete homogenization was achieved by rotating the furnace with a platinum stirrer for 6–10 h. Seed crystals were first obtained by spontaneous nucleation; after cooling the melt to the crystallization temperature, the seed was brought into contact with the melt surface, and the onset of growth was identified by the change in meniscus shape near the seed. Crystals were grown to a diameter of 20 mm at a cooling rate of 5 °C/day, and once the crystal reached a length of 20 mm, it was slightly withdrawn from the melt and cooled at 10–20 °C/h. Pulling rates and crystal dimensions are summarized in Table 2; a SBO crystal grown by this method in [10] is shown in Fig. 1.

A serious and common problem in growing borate crystals is a macroscopic opacity defect in which the crystal becomes cloudy [4]. The authors of that study succeeded in growing transparent crystals of appreciable size by correcting the stoichiometry of the starting composition (to account for volatile impurities such as water) and by maintaining a high-temperature gradient in the hot zone to suppress cellular growth. A distinctive feature of SBO crystals was their tendency to spontaneously develop domain (twin) structures during growth [11, 20–22]. For example, a Czochralski-grown SBO single crystal reported in [19] displayed an alternating domain structure of opposite polarity (space group $Pnm2_1$); upon etching, this structure was revealed as lamellae with domain walls perpendicular to the *a*-axis [21]. The domain structure was well ordered along the crystallographic *b* and *c* axes but strongly randomized along the *a*-axis. The domain formation mechanism was noted to be unknown and distinct from those observed in other systems, such as lithium niobate [38].

2.2. Kyropoulos method

In the Kyropoulos method, precise control of temperature gradients, cooling rates, and seed pulling speed enables the growth of large single crystals (typically cylindrical boules) directly from the melt. The method has been successfully

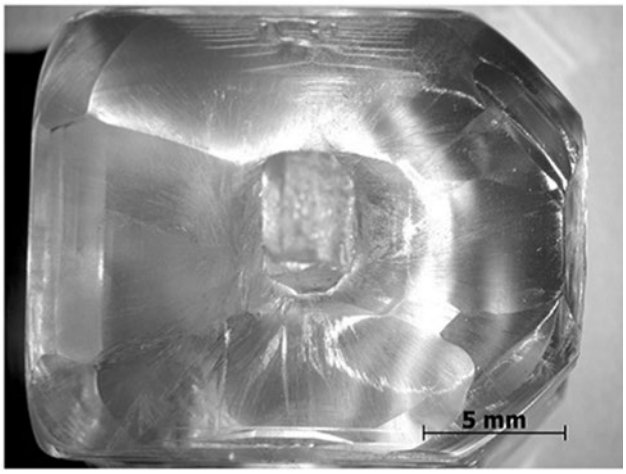

Fig. 1. Image of a crystal grown in [10]

Table 2. Conditions for growing SrB_4O_7 single crystals by the Czochralski method

$V_{\text{rotation speed of crucible}}$, rpm	V_{cooling}, °/day	V_{pulling}, mm/day	V_{pulling}, mm/h	Crystal size, mm³	Reference
–	5	2	–	20	[1]
5–20			0.1–0.3	up to 40	[4]
10	1	2.5		8×18×20	[10]
-	0.5		0.1	20×30×30	[11]
10	1	2.4		20×20×15	[19]

applied to cesium triborate CsB_3O_5 [39] and lithium triborate LiB_3O_5 [40]. The earliest report of SBO crystal growth by this technique appeared in [3], where high optical quality crystals were grown from a stoichiometric melt of $SrCO_3$ and H_3BO_3 prepared at 1030 °C. Homogenization was achieved by alternately rotating the platinum crucible in opposite directions at 30 rpm for 12–16 h. A *c*-axis-oriented seed crystal was mounted on a platinum rod, brought into contact with the melt surface at 986–987 °C, and the melt temperature was then reduced to 985 °C at 0.25 °C/day with crucible rotation maintained until the end of the growth run.

In [35], large crystals were grown over 25 days at an average pulling rate of 1.9 mm/day along the *a*-axis, yielding a boule of 328.2 g. By increasing the average pulling rate to 2.7 mm/day and reducing the growth period to 11 days, a crystal of 311.5 g was obtained (Table 3).

2.3. Micro-pulling-down method (μ–PD)

Certain applications of SBO crystals require periodic twin structures, known as QPM structures [14]. Such structures compensate for phase mismatch in second-harmonic generation (SHG) that arises during propagation in a homogeneous crystal. In QPM structures, the sign of the nonlinear optical coefficient was periodically inverted, enabling compensation of the accumulated phase mismatch and thereby enhancing SHG efficiency [41, 42]. Devices based on QPM structures provided enhanced conversion efficiency. QPM structures can be induced by poling [43, 44] and hot-pressing [45] techniques; however, these approaches were unsuitable for controlling the formation of twin boundaries in SBO crystals. By contrast, periodically poled $LiNbO_3$/$LiTaO_3$ (PPLN/PPLT) were well-established ferroelectric QPM devices fabricated by periodic polarization inversion under high electric fields [46].

Controlling twin boundary formation required the deliberate incorporation of defects, which can be accomplished by applying an electric field during crystal growth under conditions of steep temperature gradients [6, 47].

The μ–PD method, developed in Japan in the late twentieth century, was used to grow a variety of crystal types [47, 48]. It is relatively straightforward, requires no costly equipment, and operates by continuously supplying melt to the crystallization front through a micro-orifice at the bottom of the crucible. As melt exits the orifice, a pendant droplet forms under gravity, contacts an oriented seed crystal, and the growing fiber is pulled downward (Fig. 2).

The principal advantage of this approach over upward-pulling techniques is a marked reduction in gas bubble inclusions, enabling the growth of high-quality fiber crystals. Convection in the μ-PD method arises primarily from compositional non-uniformity or non-uniform melt heating.

Machida et al. [36] investigated the growth conditions for SBO fiber crystals by this method and discussed the mechanism responsible for opacity formation, using a (010)-oriented bar cut from a Czochralski-grown crystal (space group $Pnm2_1$) as the seed. Transparent crystals were obtained at pulling rates between 0.01 and 0.20 mm/min, with the clearest fibers growing at 0.01–0.03 mm/min. Figure 3 shows a fiber with segments *a*, *b*, and *c* grown at 0.03, 0.02, and 0.01 mm/min, respectively; segments *b* and *c* were transparent, whereas segment *a*, grown at 0.03 mm/min, was translucent, and the terminal portion was frequently opaque (segment *a*). These observations indicated that rates below 0.02 mm/min were most favorable for transparent fiber growth, though the origin of opaque regions warrants further investigation.

In [14, 15], growth conditions were optimized and transparent SBO single crystals were obtained by the μ–PD method under applied electric fields, with seeds pulled along the *b*-axis [15] and *c*-axis [14]. Two distinct growth mechanisms were identified in [15]: (1) at

Table 3. Conditions for growing SrB_4O_7 single crystals by the Kyropoulos method

$T_{melt,}$ °C, $t_{synthesis}$, h	$V_{rotation\ speed\ of\ crucible}$, rpm	$V_{pulling,}$ mm/day	Duration of synthesis, days	Crystal size, mm³	Reference
1030, 12–16	30	–	6	35×25×25	[3]
1002	15	1.9	25	100×30×32	[35]
1002	15	2.7	11	63×36× 9.5	[35]

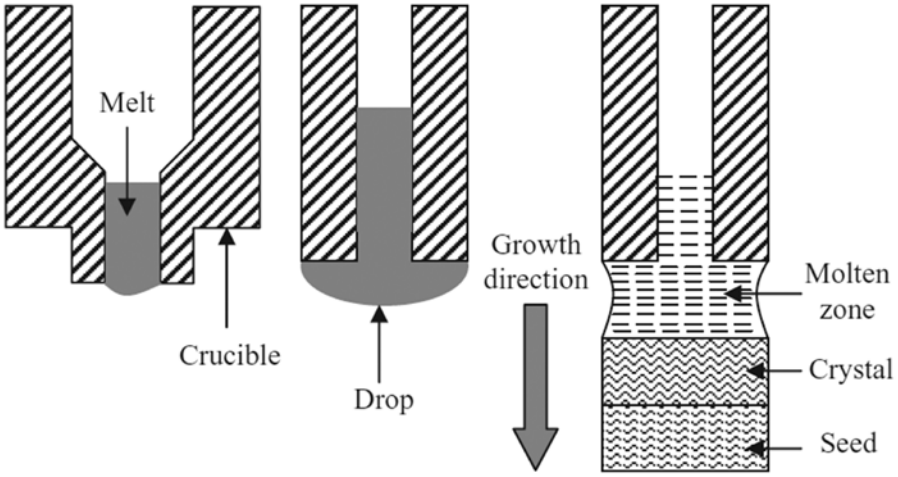

Fig. 2. Scheme of crystal growth by micro-pulling down method [49]

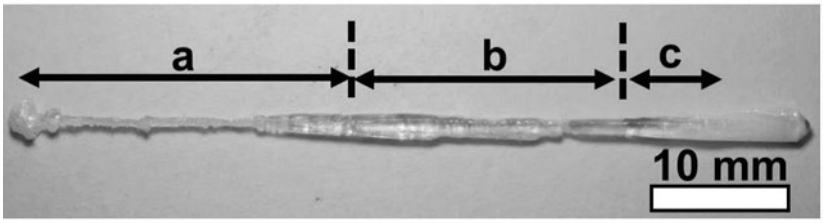

Fig. 3. SBO crystal in sections *a, b,* and *c* grown at different pulling rates according to [36]

applied fields exceeding 400 V/cm, needles of the SrB_2O_4 phase appeared within the fiber crystal, as confirmed by X-ray diffraction. These needle-shaped domains exhibited birefringence distinct from that of SBO; (2) at fields exceeding 1000 V/cm, SBO twins with a QPM structure appeared perpendicular to the crystal growth front. Owing to geometric selection, the (100) twin face could be preserved until the end of the growth run. Reversing electrode polarity in the melt, regardless of field magnitude, changed the growth front morphology from concave to convex, indicating that convection was generated perpendicular to the growth front. This convection promotes convex morphology development with increasing field strength. The absence of SrB_2O_4 needle domains above 1000 V/cm was attributed to a reduction in the diffusion boundary layer thickness and to compositional deviation with increasing voltage. Accordingly, 1000 V/cm was identified as the threshold field at which the diffusion boundary layer is completely eliminated. Under these conditions, no interface between the seed and the grown crystal was observed.

In [15], the authors also examined the growth of SBO fiber crystals along the *c*-axis under $E < 1000$ V/cm and $E = 1000$ V/cm, confirming that the crystallographic seed orientation was preserved in the grown crystal. In this configuration, neither SrB_2O_4 needle domains nor twin boundaries were observed; however, the interior of the fibers was not homogeneous. Fibers grown at 800 V/cm were slightly opaque due to rough surfaces. Even at low fields, SrB_2O_4 domains did not form, and the growth front morphology in the absence of an applied field was concave, which is consistent with the result for *b*-axis growth reported in [14]. Since the rate-limiting step in melt growth was the dissipation of latent heat, the resulting heat flux determined growth front morphology. These observations suggested that latent heat of crystallization accumulated near the center of the growth interface. Surface morphology inversion was observed, with a particularly pronounced convex shape at 1000 V/cm, demonstrating that alternating the applied electric field forcibly generates convection perpendicular to the growth front. Unlike the previous study [14], twin boundaries perpendicular to the growth

front did not form under these conditions. It was concluded that *c*-axis growth is not favorable for twin formation. Furthermore, it was found that alternating applied fields generate convection perpendicular to the growth front. This contradicts the conventional understanding of the μ–PD growth mechanism, which is not associated with the onset of convection, even during the application of electric fields [13, 50, 51]. It was therefore concluded that the choice of growth axis was not the determining factor for twin formation; rather, the selection of growth conditions was paramount [14]. According to [15], only those domains in which the preferred growth faces were fully oriented perpendicular to the growth front survive.

2.4. Modified top-seeded solution growth (TSSG) method

The successful growth of large borate crystals by the TSSG method has been reported previously [52–54]. In [52], high-quality CLBO crystals were grown using a conventional vertical furnace in the TSSG configuration, in which thorough mixing was achieved by a stationary propeller combined with crucible rotation. The crystal was grown over 14 days by reducing the temperature from 842.5 to 841.8 °C at 0.05–0.1 °C/day. Counter-rotation of the crystal relative to the crucible at a moderate growth rate of approximately 2 mm/day improved crystalline quality by reducing local stagnation of solute supersaturation [53]. Under temperature oscillations induced by a rotating thermal field, through which heat and mass transport at the crystallization front were controlled, high-quality crystals could be obtained [54].

This method was applied to the growth of Eu^{2+}/Li^{+}-doped SBO crystals with well-developed facets, free of macrodefects and cracks [37]. In [6], high-quality SBO crystals were grown in a three-zone vertical furnace (Fig. 4) from both a boron-rich solution (Sr:B = 17:80) and a stoichiometric melt. SBO powder was prepared by solid-state reaction from $SrCO_3$ and B_2O_3 at 940 °C for 24 h and subsequently melted above 1000 °C. A *c*-axis-oriented seed crystal was rotated at 5 rpm with continuous reversal every 5 minutes while the crucible counter-rotated at 15 rpm. Three pulling rates, 11.4, 6.0, and 2.0 mm/day along the *a*-axis, were used for growth from the boron-rich solution over periods of 42, 72, and 96 h, respectively. SBO crystal growth from this solution proceeded under near-thermal-equilibrium supersaturation conditions, which favors high-quality output; a growth rate below 2 mm/day was found to be most suitable [6]. When growing from the stoichiometric melt, air was supplied at 3 L/min (Fig. 4) to prevent seed dissolution (seed cooling technique). SBO crystals were grown near the melting point at an average rate of 0.9 mm/day along the *a*-axis. After 20 days, the crystal was lifted from the melt and cooled to room temperature at 6.7 °C/h. Polished SBO crystals grown from the stoichiometric melt are shown in Fig. 5.

3. Mechanical properties

The surface optical damage threshold was determined for SBO and PbB_4O_7 (PBO) crystals cut along the principal optical plane XZ, and for

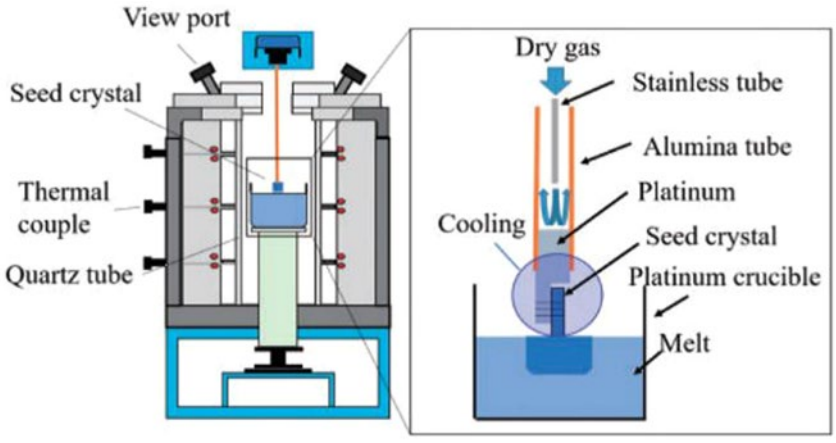

Fig. 4. Schematic diagram of the TSSG furnace and the seed cooling mechanism according to [6]

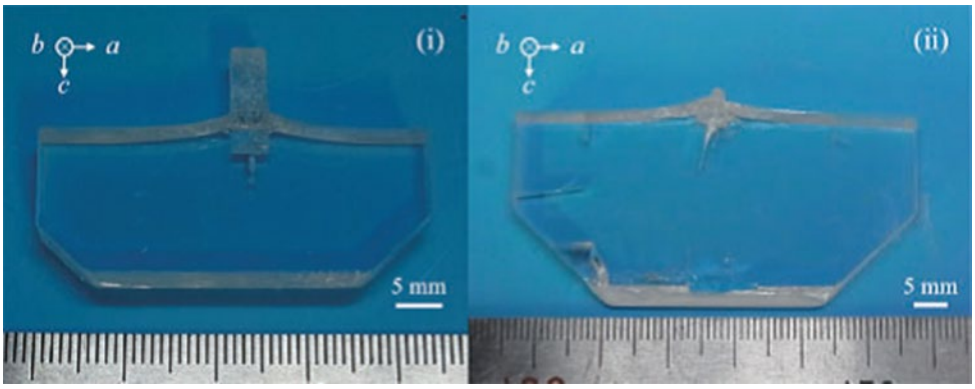

Fig. 5. Polished SBO crystals from stoichiometric melt with dimensions (*a*×*b*×*c*) (i) 42×8×18 mm³ and (ii) 60×9.2×28 mm³ according to [6]

LiB_3O_5 (LBO) and BaB_2O_4 (BBO) crystals cut at the SHG phase-matching angle [1]. Optical damage was assessed from burn marks produced by a high-power Nd:YAP laser (λ = 1.079 μm) with a Gaussian beam profile and a pulse duration of 15 ns.

Microhardness measurements on SBO and PBO crystals were performed along the principal optical axis directions (Table 4).

As seen from Table 4, the microhardness of SBO exceeded that of PBO by a significant margin and was more than twice that of LBO [1]. The surface optical damage threshold of SBO was essentially equal to that of α-BBO [56], more than twice that of LBO, and three times that of PBO. Among borate crystals, only β-BBO and LTBO (which show some of the highest reported damage thresholds) surpassed SBO in this respect.

In the structure of α-SBO, both crystallographically independent boron atoms are four-coordinate, although the presence of BO_4 tetrahedra is usually accompanied by BO_3 triangles [8–10, 16]. Unusually, one oxygen atom is shared simultaneously by three BO_4 tetrahedra, with an average B–O bond length of approximately 1.55 Å. In conventional borate tetrahedra, the average B–O distance is about 1.47 Å. The primary structural units are non-planar six-membered ring anions $(B_3O_9)^{9-}$, each composed of three $(BO_4)^{3-}$ groups. These ring anions form chains oriented along [001], which are linked through bridging oxygen atoms to form layers. The layers are in turn interconnected into a three-dimensional borate–oxygen framework with strontium atoms occupying the interstices (Fig. 6).

This structural arrangement imparts to strontium tetraborate characteristics typical of layered borate structures, including a tendency toward perfect cleavage. An indentation study of fracture toughness [12] revealed imperfect cleavage along the (100) plane (space group $Pnm2_1$), with a cleaved surface morphology consisting of steps parallel to (100). Cleavage is uncommon in framework-type borates owing to strong covalent B–O bonds. Therefore, under

Table 4. Optical damage threshold and microhardness of borate crystals

Crystal	ρ, g/cm³	I_d, W/cm²	*Hkx*, kg/mm²	*Hky*, kg/mm²	*Hkz*, kg/mm²
SBO [17]	4.011	14.7	1751	1461	1345
LBO [55]	2.47	6.0	768	755	607
LBO [1]		9.3			
SBO [1]	4.011	14.7	1750	1460	1350
PBO [1]	5.852	3.6	1270	1170	1190
BBO [1]		4.0			
LTBO [56]		32.2			
α-BBO [56]		14.5			
β-BBO [56]		30.9			

mechanical stress, SBO crystals cleave along borate–oxygen layers lying in the (100) plane. It was suggested that crack propagation within the (010) and (001) planes was associated with the breaking of bridging oxygen bonds and the disruption of boron–oxygen chains. The crack toughness values in these planes were notably high, $K_c^{(010)}$ = 2.83 and $K_c^{(001)}$ = 2.41 MPa·m$^{1/2}$, comparable to that of Al_2O_3 (K_c = 2.9 MPa·m$^{1/2}$) [57]. The data reported in [57] were consistent with those in [17], where the Mohs hardness of SBO crystals was given as 9.

4. Optical properties

4.1. Optical and electro-optical investigations

Comprehensive investigations of the optical and nonlinear optical properties of SBO (SBO) and PbB_4O_7 (PBO) crystals were carried out by Oseledchik et al. [1]. Transmission measurements on crystalline samples were performed using a VUV spectrometer and a Specord instrument covering the visible and infrared spectral ranges. Propagation of the light beam along one of the principal crystal axes, with angular deviation below one arcminute, enabled refractive index determination with an accuracy of 10^{-4}. The small difference between the principal refractive indices of SBO and PBO demonstrated the impossibility of phase-matched SHG and sum-frequency generation in these crystals. The short-wavelength transparency cutoff of SBO was found to extend into the VUV, with a transparency range of 130–3200 nm; that of PBO was 235–4000 nm. According to [3], electro-optic coefficients of SBO measured at selected wavelengths, for example, at 5320 Å, revealed somewhat larger differences between n_x and n_z than those originally reported by Oseledchik et al. [1]. Calculations in [3] confirmed the conclusion that SBO exhibited extremely low birefringence, which was insufficient for phase matching in SHG processes. Some discrepancies were also noted between VUV and infrared spectrometer measurements, the latter yielding a transparency range of 120–4000 nm. The material was found to be transparent at wavelengths below 120 nm, which is a remarkably unusual property. In addition, two absorption peaks were identified in the VUV region at λ = 150–240 nm, the origin of which remains to be clarified.

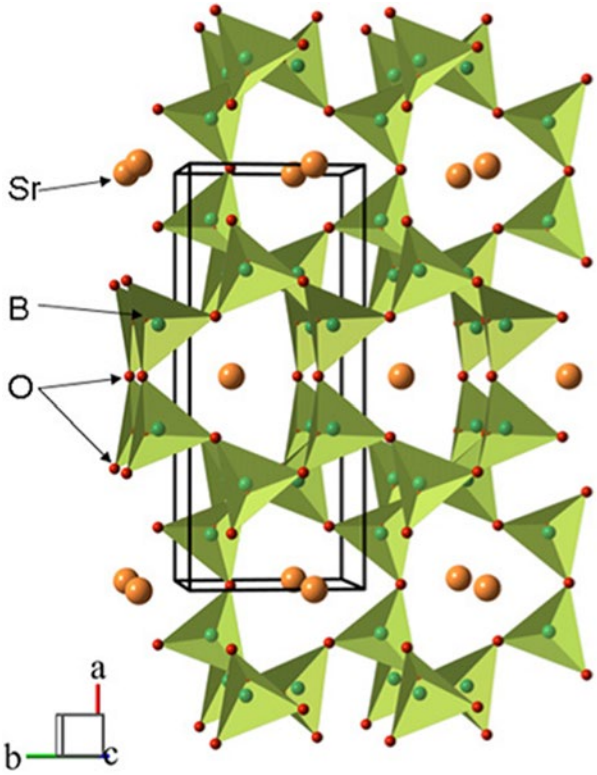

Fig. 6. Crystal structure of SrB_4O_7 (sp. gr. $Pmn2_1$) according to [10]

Boghati et al. [18], in a study of the electro-optic and electrostrictive properties of SBO and PbB_4O_7, noted their structural isotypism. Measurements were performed on three SBO samples in different orientations by combining transmission and reflection geometries for a linearly polarized light wave relative to an applied electric field. The electro-optic and electrostrictive effects in SBO were smaller than those in its structural analog PBO [58], a difference most pronounced for the maximum longitudinal and transverse effects. To assess the suitability of SBO for electro-optic applications, Oseledchik et al. [1] determined the elements r_{ij} of the electro-optic tensor matrix. Since SBO and PBO belong to the orthorhombic system with point group symmetry *mm*2 [1], samples were cut along the principal optical planes and at 45° in the XZ and YZ planes. An electric field was applied both transverse to and along the direction of light propagation, and the rotation of the plane of polarization was measured. The half-wave voltage was found to be no less than 50 kV for all possible SBO crystal orientations. Accordingly, the electro-optic coefficients r_o were

estimated to be no greater than $5 \cdot 10^{-3}$ m/V. These values were too small for practical application in electro-optic devices.

4.2. Nonlinear optical properties

In [1, 17], the transparency ranges, effective nonlinear optical coefficients, and laser-induced surface damage thresholds of SBO and PbB_4O_7 were determined. Second-harmonic generation (SHG) of Nd:YAG laser radiation at λ = 1064 nm was investigated using SBO powder samples with different mean particle sizes [17]. The results were compared with those obtained for well-established nonlinear optical materials such as potassium titanyl phosphate (KTP) and lithium triborate (LBO). The relative SHG intensity as a function of particle size I(d) indicated that the effective nonlinear coefficient of SBO was of the same order of magnitude as that of KTP: d_{eff}(SBO) ~ d_{eff}(KTP); and significantly higher than that of LBO: d_{eff}(SBO) > d_{eff}(LBO). The observed dependence of SHG intensity on particle size confirmed the absence of phase matching at λ = 1064 nm. With increasing particle size, a decrease in SHG intensity was observed, while the initial slope of the curve at small particle sizes was proportional to the effective nonlinear coefficient. Despite the absence of phase-matching, incoherent nonlinear optical processes in SBO can proceed with good efficiency owing to the large nonlinear coefficient and long coherence length.

The authors of [1] observed the generation of the third and fourth harmonics simultaneously in a single crystal. The third harmonic was obtained by summing the first and second harmonics, and the fourth harmonic was obtained by doubling the second harmonic.

Irregular domain structures that formed spontaneously during SBO crystal growth [19–22] gave rise to QPM, enabling efficient nonlinear optical conversion [59]. These structures constituted a one-dimensional nonlinear photonic crystal (NPC) [24] with a broad spectrum of reciprocal lattice vectors, thereby supporting efficient frequency generation over a wide spectral range. Frequency-doubling experiments using a femtosecond Ti:sapphire laser in the nonlinear diffraction regime on the domain structure of SBO were reported in [59]. This laser served as the pump source, generating pulses with an energy of 12.5 nJ and durations of 40–100 fs. Tunable second-harmonic output was obtained across the spectral range 355–510 nm, with a maximum SHG conversion efficiency of 1.9 %. The spectral bandwidth of the second-harmonic radiation was narrowed by no more than 1–20 %. These results indicated the promise of domain-structured SBO for UV applications, including use as the basis of an autocorrelator for ultrashort pulse diagnostics.

The conversion of coherent radiation into the VUV spectral region is of considerable interest for a wide range of applications. Trabs et al. [60] exploited random QPM (RQPM) in SBO crystals to investigate tunable coherent radiation in this region. It was found that RQPM in SBO enabled second-harmonic generation down to 121 nm, representing one of the shortest wavelengths reported for second-order nonlinear optical processes in solid-state materials. This opened the way for coherent radiation generation in the deep VUV or for temporal characterization of ultrashort pulses via an inverse second-order nonlinear process. Compared with non-phase matched processes, a signal enhancement exceeding four orders of magnitude was observed. The reported SHG conversion efficiency of ~10^{-5}, driven by a femtosecond Ti:sapphire laser, corresponded to single-pulse energies comparable to those associated with sixth-harmonic generation [60].

Ma et al. [61] employed density functional theory to calculate the effect of uniaxial strain along the [100] direction on the birefringence and second-order susceptibility of SBO crystals (space group $Pmn2_1$). A 10% axial compressive or tensile strain was found to increase the birefringence by a factor of 13–16 relative to the unstrained crystal, simultaneously enhancing the possibility of UV phase-matched SHG, promoting deeper UV absorption, and increasing the second-order susceptibility.

4.3. Elastic, piezo-optical, and acousto-optical properties

The acousto-optic (AO) effect is the diffraction of light by dielectric permittivity inhomogeneities induced by acoustic waves propagating in a transparent medium, which has found numerous

scientific and technological applications. Devices such as modulators, deflectors, and filters exploit this effect to control and process light beams for the characterization of electromagnetic or acoustic waves [33, 62–65]. The efficiency of such devices depended critically on the interaction geometry, i.e., the directions of propagation and polarization of the electromagnetic and acoustic waves, making it essential to identify the directions that maximize the AO effect [66, 67]. Crystalline materials for such devices were selected on the basis of a combination of properties.

Table 5 lists the optical parameters of several borate crystals. Among the borates surveyed, the highest AO figure of merit M_2 was exhibited by α- and β-BaB_2O_4, which also displayed one of the highest optical damage thresholds and the widest transparency ranges, making them well suited for AO device applications. LTBO crystals showed the highest optical damage resistance. The AO figure of merit reported for PBO ($M_2 = 0.66 \cdot 10^{-18}$ s^3/g) was considered too small for practical AO device use by the authors of [64].

Complete matrices describing the acoustic, elastic, and piezo-optical properties of SBO crystals were obtained in [33]. The highest AO figure of merit, $M_2 = (10.4 \pm 6.6) \cdot 10^{-15}$ s^3/kg, was found for interaction with the slowest acoustic wave, propagating at 5,470 ± 80 m/s. Since α-SBO is transparent to 130 nm, all optical parameters are expected to increase in this spectral region due to dispersion, suggesting that SBO may be an efficient material for AO devices operating in the deep UV. A small anisotropy of acoustic wave velocities was observed, with longitudinal wave velocities exceeding those of transverse waves. The photoelastic coefficients and their anisotropy may significantly influence the AO efficiency. Experimental investigations of diffraction and the piezo-optic effect in the VUV and deep UV were associated with considerable practical difficulties [66]. Consequently, the photoelastic and piezo-optic coefficients reported in [33] for α-SBO and PBO were estimated approximately, without accounting for the Poisson effect [66].

According to [1, 3], the structure of α-SBO was based on a three-dimensional network built exclusively from BO_4 tetrahedra, with oxygen atoms occupying certain structural positions where they were three-coordinate with respect to boron. This resulted in an exceptionally high atomic density compared with other borates [5, 33, 64]. Zinenko et al. [68] used Raman scattering to measure the cutoff frequencies of lattice vibrations in α-SBO crystals. They calculated the complete spectrum of lattice vibrations, elastic and piezoelectric constants, Born effective charges, and the high-frequency dielectric permittivity, all of which showed satisfactory agreement with experimental data. To account for the domain structure of α-SBO, a model based on a hypothetical centrosymmetric paraphase with space group *Pnnm* was proposed. The assumption of a nonpolar hypothetical paraphase enabled calculation of the spontaneous polarization in the experimentally observed structure. The resulting value of 114 μC/cm^2 was several times larger than the spontaneous polarization of the classical ferroelectric $BaTiO_3$.

Paraelectric materials with low birefringence (such as arsenide and nitride semiconductors) were well suited for wavelength conversion devices, combining high optical nonlinearity comparable to that of ferroelectrics with a wide transparency window and high resistance to optical damage [69]. The authors of [69] proposed a monolithic microresonator wavelength-conversion device free of domain-inverted structures, fabricated from paraelectric materials and applicable to any optically nonlinear crystal. In addition, the proposed device offered several advantages, including a larger nonlinear coupling coefficient than conventional mode-phase matched SHG microring resonators, efficient light extraction, and compact dimensions.

An ultracompact microresonator wavelength-conversion device based on the paraelectric crystal SBO, generating coherent radiation in the deep UV at 234 nm, was developed in [70]. Owing to its wavelength-conversion potential and transparency to 130 nm, this device was expected to find application in bacterial disinfection and viral inactivation. For compact and versatile solid-state coherent light sources in the VUV, a vertical microresonator based on SBO for SHG at 199 nm has been proposed through modification of the distributed Bragg reflector material and optimization of the device structure for pulsed laser pumping [71]. Conventional crystals used

Table 5. Optical parameters of borate crystals as acousto-optic materials

Phase	Transparency range, nm	Refractive indices	Modulus of elasticity, $1 \cdot 10^{11}$ Pa	Photoelasticity coefficients (elasto-optical)	M_2, 10^{-15} s^3/kg	Piezoelectric coefficients, s/m^2	Permittivity
α-SrB_4O_7 (SBO)	130–3200 [1] 120–4000 [3]	λ = 623.8 nm n_x = 1.721 n_y = 1.722 n_z = 1.723 [3]			0.36 [66] 10.4 [33]	Piezoelectric voltage constant ×10^{-8}, V/m h_{33} = 7.8 h_{15} = 5.7 h_{24} = 22.9 [66]	ε_{11} = 3.01 ε_{22} = 2.97 ε_{33} = 3.03 [68]
α-SrB_4O_7 (SBO)		λ = 632.8 nm n_1 = 1.7333 n_2 = 1.7323 n_3 = 1.7356 [33]	c_{11} = 3.04; c_{12} = 0.7; c_{13} = 0.49; c_{22} = 2.68; c_{23} = 0.55; c_{33} = 3.78; c_{44} = 1.39; c_{55} = 1.20; c_{66} = 1.33 [33]	p_{11} = -0.04; p_{12} = 0.15; p_{13} = 0.16; p_{21} = 0.15; p_{22} = –0.001; p_{23} = 0.15; p_{31} = 0.19; p_{32} = 0.16; p_{33} = –0.08; p_{44} = –0.05; p_{55} = –0.06; p_{66} = - 0.06; [66]	0.58 [67] 0.63 [62]	s/m^2 e_{15} = 0.71; e_{24} = 0.22; e_{31} = 1.23; e_{32} = 1.03; e_{33} = 1.92 [66]	50 MHz $\varepsilon_{11} = \varepsilon_{33}$ = 10.1 ε_{22} = 9.8 [33, 66]
PbB_40_7 (PBO)	235–4000 [1]	n_1 = 1.9326 n_2 = 1.9275 n_3 = 1.9309 [33]	c_{11} = 3.42; c_{12} = 9.6; c_{13} = 0.67; c_{22} = 3.04; c_{23} = 0.64; c_{33} = 3.67; c_{44} = 1.35; c_{55} = 1.17; c_{66} = 1.29 [33]		2.9 [33] 0.00066 [64]		
α-BaB_2O_4 (α-BBO)	280-2800 [56]	n_0 = 1.6670 n_e = 1.5280 [56]	c_{11} = 1.19; c_{12} = 0.53; c_{13} = 0.56; c_{14} = 0.05; c_{33} = 0.38; c_{44} = 0.05; c_{66} = 0.32 [56]		54.5 [56]		
β-BaB_2O_4 (β-BBO)	280-3220 [56]	n_0 = 1.6673 n_e = 1.5500 [56]	c_{11} = 1.23; c_{12} = 0.60; c_{13} = 0.49; c_{14} = 0.12; c_{33} = 0.53; c_{44} = 0.07; c_{66} = 0.31 [56]	p_{44} = –0.078 [56]	49.4 [56]		
LB_3O_5 (LBO)	160-3200 [55]	λ = 532 nm n_1 = 1.5789 n_2 = 1.6070 n_3 = 1.6214 λ = 1064 нм n_1 = 1.5652 n_2 = 1.5615 n_3 = 1.6065 [55]					
$Li_2B_4O_7$ (LB4)	250-3200 [56]	n_0 = 1.6084 n_e = 1.5516 [56]	c_{11} = 1.31; c_{12} = 0.33; c_{13} = 0.55; c_{33} = 0.61; c_{44} = 0.55; c_{66} = 0.47 [56]	p_{44} = 0.0498 [56]	0.55 [56]		

for VUV generation (CLBO (237 nm) and β-BBO (205 nm)) cannot produce VUV radiation without sum-frequency generation, which substantially increased system complexity [72]. The proposed device may ultimately prove to be the sole high-efficiency VUV coherent light source capable of replacing such complex pumping systems.

5. Conclusion

The majority of publications on strontium tetraborate have focused on α-SBO. This reflected the fact that conventional growth of β-SBO from the melt under conditions of small undercooling was not feasible. It was established in [73] that above 800 °C the β-phase began to convert at the crystal surface to α-SBO, and by 950 °C the transformation to the α-phase was complete and irreversible. Growth of β-SBO crystals was therefore possible only from a strongly undercooled melt, which presented a considerable challenge. The difficulty arose from the high melt viscosity and the formation of secondary phases, α-SBO, β-SBO, and $Sr_4B_{14}O_{25}$ crystals, as well as spherulites of an unidentified metastable phase. The practical promise of strontium tetraborate created a demand for large, high-quality transparent crystals. Because SBO melts congruently, crystals exceeding 20 mm can be grown directly from the melt. Methods employed for this purpose included the Czochralski and Kyropoulos techniques and their variants, μ–PD and TSSG methods. Of these, the Czochralski method was the most widely used.

A persistent and serious problem in the growth of borate crystals was optical opacity caused by the high viscosity of the melt and cracking during crystallization. These drawbacks can be mitigated by adjusting the stoichiometric composition, precisely controlling the temperature gradients in the hot zone, and optimizing both the cooling rate and the pulling speed.

SBO crystals can spontaneously develop domain (twin) structures during growth. An alternating domain structure of opposite polarity has been obtained in this way, manifested as lamellae with domain walls perpendicular to the *a*-axis [20, 21]. The mechanism of domain formation remained unknown and differed from those observed in crystals of other compound classes. To control twin-boundary formation, the deliberate introduction of defects through application of an electric field during growth under high-temperature gradient conditions has been proposed.

The principal advantage of the μ–PD method over conventional upward-pulling techniques was a reduction in gas inclusions, enabling the growth of high-quality fiber crystals. According to the conventional understanding of μ–PD crystal growth, convection did not arise during growth, even when electric fields are applied. However, it has been found that alternating applied field voltages induce convection perpendicular to the growth front [14]. This convection in the μ–PD method was attributed to non-uniform heating and compositional inhomogeneity of the melt, which was inconsistent with the conventional picture. Consequently, the growth conditions, rather than the choice of crystallographic axes as twin growth faces, were the critical factor governing the process. It has been shown that only domains whose preferred growth faces were fully oriented perpendicular to the growth front survived. The formation of irregular domain structures in SBO crystals gave rise to random QPM (RQPM), enabling efficient nonlinear optical conversion. SHG experiments using a femtosecond Ti:sapphire laser operating in the nonlinear diffraction regime on the SBO domain structure demonstrated tunable second-harmonic output over the spectral range 355–510 nm, with the pump laser delivering pulses of 12.5 nJ energy and 40–100 fs duration. This result highlighted the potential of domain-structured SBO crystals in the UV region for ultrashort-pulse characteristic. RQPM in SBO has also been exploited for tunable coherent emission across this spectral range [60]. It was found that RQPM in SBO supports SHG down to 121 nm, making it applicable to coherent light generation in the deep VUV. Compared with non-phase-matched conversion, a signal gain exceeding four orders of magnitude was achieved. The resulting SHG conversion efficiency of ~10^{-5}, pumped by a Ti:sapphire femtosecond laser, yielded single-pulse energies corresponding to the sixth harmonic. SBO crystals were characterized by thermal stability, high microhardness, a high surface laser-induced damage threshold, and negligible hygroscopicity. Among borates, SBO

was surpassed in laser-induced damage threshold only by β-BBO and LTBO, which exhibited some of the highest damage thresholds reported for this material class.

Complete tensor matrices describing the acoustic, elastic, and piezo-optic properties of SBO crystals have been determined. The highest acousto-optic figure of merit, $M_2 = 10.5 \cdot 10^{-15}$ s^3/kg, was achieved through interaction with the slowest acoustic mode, which propagates at 5,470 ± 80 m/s. Since α-SBO was transparent down to 130 nm, all optical parameters were expected to increase in this range due to dispersion, suggesting that this material may perform effectively in acousto-optic devices operating in the deep UV. The unusually high atomic density of α-SBO relative to other borates was a consequence of its structure, which consisted exclusively of BO_4 tetrahedra with oxygen atoms occupying certain structural sites in threefold coordination with boron. To account for the domain structure of α-SBO, a model based on a hypothetical centrosymmetric paraphase with space group *Pnnm* has been proposed. This non-polar paraphase model enabled calculation of the spontaneous polarization in the experimentally observed structure, yielding a value of 114 μC/cm^2, which was several times larger than the polarization of the classical ferroelectric $BaTiO_3$. An ultracompact microresonator device for wavelength conversion based on paraelectric SBO has already been developed, producing coherent radiation in the deep UV at 234 nm. With its high wavelength-conversion potential and transparency extending to 130 nm, this device was expected to find application as a tool for bacterial disinfection and viral inactivation. A vertical microresonator based on SBO for SHG at 199 nm has been proposed as a replacement for complex laser pumping systems, and may ultimately represent the only highly efficient source of coherent VUV light.

Author contributions

The authors contributed equally to this article.

Conflict of interests

The authors declare that they have no known competing financial interests or personal relationships that could have influenced the work reported in this paper.

References

1. Oseledchik Y. S., Prosvirnin A. L., Pisarevskiy A. I., … Selevich A. F. New nonlinear optical crystals: strontium and lead tetraborates. *Optical Materials*. 1995;4: 669–674. https://doi.org/10.1016/0925-3467(95)00027-5

2. Petrov V., Noack F., Shen D., … Alex V. Application of the nonlinear crystal SrB_4O_7 for ultrafast diagnostics converting to wavelengths as short as 125 nm. *Optics Letters*. 2004;29(4): 373–375. https://doi.org/10.1364/OL.29.000373

3. Pan F., Shen G., Wang R., Wang X., Shen D. Growth, characterization and nonlinear optical properties of SrB_4O_7 crystals. *Journal of Crystal Growth*. 2002;241: 108–114. https://doi.org/10.1016/S0022-0248(02)00873-4

4. Komatsu R., Kawano H., Oumaru Z., Shinoda K., Petrov V. Growth of transparent SrB_4O_7 single crystal and its new applications. *Journal of Crystal Growth*. 2005;275: 843–847. https://doi.org/doi:10.1016/j.jcrysgro.2004.11.122

5. Zaitsev A. I., Aleksandrovskii A. S., Zamkov A. V., Sysoev A. M. Nonlinear optical, piezoelectric, and acoustic properties of SrB_4O_7. *Inorganic Materials*. 2006;42(12): 1360–1362. https://doi.org/10.1134/s0020168506120132

6. Tanaka Y., Shikata K., Murai R., …Yoshimura M. Growth of high-quality transparent SrB_4O_7 single crystals with high degradation resistance for DUV laser application. *Applied Physics Express*. 2018;11: 125501. https://doi.org/10.7567/APEX.11.125501

7. Cao Z., Wei X., Zhao L., Chen Y., Yin M. Investigation of SrB_4O_7: Sm^{2+} as a multimode temperature sensor with high sensitivity. *ACS Applied Materials & Interfaces*. 2016;8(50): 34546–34551. https://doi.org/10.1021/acsami.6b10917

8. Krogh-Moe J., Magneli A., Seip R., Seip H. M. The crystal structure of strontium diborate, $SrO{\cdot}2B_2O_3$. *Acta Chemica Scandinavica*, 1964;18: 2055–2060. https://doi.org/10.3891/acta.chem.scand.18-2055

9. Stein W.-D., Liebertz J., Becker P., Bohatrý L., Braden M. Structural investigations of the tetraborates MB_4O_7 (M = Pb, Sr, Ba). *European Physical Journal B*. 2012;85: 236. https://doi.org/10.1140/epjb/e2012-21062-y

10. Atuchin V. V., Kesler V. G., Zaitsev A. I., … Ignatova N. Y. Electronic structure of α-SrB_4O_7: experiment and theory. *Journal of Physics: Condensed Matter*. 2013;25: 085503. https://doi.org/10.1088/0953-8984/25/8/085503

11. Zaitsev A. I., Radionov N. V., Cherepakhin A. V., Vasiliev A. D., Zamkov A. V. Morphology of the polar twin structure in Czochralski grown α-SrB_4O_7 crystals. *Journal of Crystal Growth*. 2015;416: 17–20. https://doi.org/10.1016/j.jcrysgro.2015.01.004

12. Dolzhenkova E. F., Baumer V. N., Tolmachev A. V., Oseledchik Yu. S. On the nature of fracture of SrB_4O_7 and PbB_4O_7 single crystals. *Crystallography Reports*. 2007;52(5): 889–893. https://doi.org/10.1134/s1063774507050197

13. Block S., Perloff A., Weir C. E. The crystallography of some M^{2+} borates. *Acta Crystallographica*. 1964;17: 314-315. https://doi.org/10.1107/S0365110X64000767

14. Inaba S., Ishibashi R., Asakawa H., Machida T., Hamada Y., Komatsu R. Effects of the application of electric fields on the growth of SrB_4O_7 crystals by the micro-pulling-down method. *Crystal Growth & Design*. 2020;21(1): 86–93. https://doi.org/10.1021/acs.cgd.0c00828

15. Ishibashi R., Asakawa H., Komatsu R. Growth of SrB_4O_7 crystal fibers along the c-axis by micro-pulling-down

method. *Crystals*. 2021;11: 987. https://doi.org/10.3390/cryst11080987

16. Perloff A., Block S. The crystal structure of the strontium and lead tetraborates, $SrO{\cdot}2B_2O_3$ and $PbO{\cdot}2B_2O_3$. Acta *Crystallographica*. 1966;20: 274–279. https://doi.org/10.1107/S0365110X66000525

17. Oseledchik Y. S., Prosvirnin A. L., Starshenko V. V., … Krikunov S. A. Crystal growth and properties of strontium tetraborate. *Journal of Crystal Growth*. 1994;135(1-2): 373–376. https://doi.org/10.1016/0022-0248(94)90767-6

18. Bohaty L., Liebertz J., Stähr S. Strontiumtetraborat SrB_4O_7: einkristallzüchtung, elektrooptische und elektrostriktive eigenschaften. *Zeitschrift für Kristallographie*. 1985;172(1-2): 135–138. https://doi.org/10.1524/zkri.1985.172.1-2.135

19. Aleksandrovsky A. S, Vyunishev A. M, Zaitsev A. I., Zamkov A. V., Arkhipkin V. G . Detection of randomized nonlinear photonic crystal structure in a non-ferroelectric crystal. *Journal of Optics A: Pure and Applied Optics*. 2007;9: S334–S338. https://doi.org/10.1088/1464-4258/9/9/S08

20. Zaitsev A. I., Aleksandrovsky A. S., Vasiliev A. D., Zamkov A. V. Domain structure in strontium tetraborate single crystal. *Journal of Crystal Growth*. 2008;310(1): 1–4. https://doi.org/10.1016/j.jcrysgro.2007.09.037

21. Aleksandrovsky A. S., Vyunyshev A. M., Shakhura I. E., Zaitsev A. I., Zamkov A. V. Random quasi phase matching in nonlinear photonic crystal structure of strontium tetraborate. *Physical Review A*. 2008;78: 031802. https://doi.org/10.1103/PhysRevA.78.031802

22. Aleksandrovsky A. S., Vyunyshev A. M., Slabko V. V., Zaitsev A. I., Zamkov A. V. Tunable femtosecond frequency doubling in random domain structure of strontium tetraborate. *Optics Communications*. 2009;282(11): 2263–2266. https://doi.org/10.1016/j.optcom.2009.02.070

23. Vasiliev A. D., Cherepakhin A. V., Zaitsev A. I. The trigonal polymorph of strontium tetraborate, β-SrB_4O_7. *Acta Crystallographica Section E: Crystallographic Communications*. 2010;66: i48. https://doi.org/10.1107/S1600536810019069

24. Berger V. Nonlinear photonic crystals. *Physical Review Letters*. 1998;81: 4136–4139. https://doi.org/10.1103/PhysRevLett.81.4136

25. Baudrier-Raybaut M., Haïdar R., Kupecek Ph., Lemasson Ph., Rosencher E. Random quasi-phase-matching in bulk polycrystalline isotropic nonlinear materials. *Nature*. 2004; 432(7015), 374–376. https://doi.org/10.1038/nature03027

26. Popov P. A., Solomennik V. D., Zaitsev A. I., Zamkov A. V., and Gorev M. V. Heat conductivity and thermal expansion of crystal strontium tetraborate SrB_4O_7. *Doklady Physics*. 2012;57(2): 54–56. https://doi.org/10.1134/S1028335812020036

27. Moiseev N. V., Popov P. A., Solomennik V. D., Zaitsev A. I., and Cherepakhin A. V. Heat capacity and thermodynamic properties of crystalline SrB_4O_7. *Inorganic Materials*. 2012;48(5): 504–507. https://doi.org/10.1134/S0020168512050123

28. Witzman H. and Beulich W. Zur bildung wasserfrier strontiumborate ein beitrag zum zustandsdiagramm des systems $SrO\text{-}B_2O_3$. *Zeitschrift für Physikalische Chemie*. 1964;225(5–6): 336–341. https://doi.org/10.1515/zpch-1964-22535

29. Kudrjavtcev D. P., Oseledchik Yu. S., Prosvirnin A. L., Svitanko N. V. Growth of a new strontium borate crystal $Sr_4B_{14}O_{25}$. *Journal of Crystal Growth*. 2003;254: 456–460. https://doi.org/10.1016/S0022-0248(03)01207-7

30. Zaitsev A. I., Zamkov A. V., Koroleva N. S., Molokeev M. S., and Cherepakhin A. V. Phase Formation upon Crystallization of $SrO{\cdot}2B_2O_3$ Glasses. *Crystallography Reports*. 2011;56(1): 44–51. DOI: 10.1134/S1063774511010263

31. Asakawa H., Machida T., Inaba S., … Komatsu R. Growth of SrB_4O_7 crystal fibers with near-stoichiometric composition by the micro-pulling-down method. *Crystal Growth & Design*. 2019;19: 6258–6265. https://doi.org/10.1021/acs.cgd.9b00732

32. Polyakova I. G., Litovchik E. O. Crystallization of glasses in the $SrO–B_2O_3$ system. *Glass Physics and Chemistry*. 2008;34(4): 369–380. https://doi.org/10.1134/S1087659608040056

33. Martynyuk-Lototska I., Dudok T., Mys O., Vlokh R. Elastic, piezooptic and acoustooptic properties of SrB_4O_7 and PbB_4O_7 crystals. *Optical Materials*. 2009;31(4): 660–667. https://doi.org/10.1016/j.optmat.2008.06.020

34. Tanaka Y., Murai R., Takahashi Y., Sugita T., … Yoshimura M. High surface laser-induced damage threshold of SrB_4O_7 single crystals under 266-nm (DUV) laser irradiation. *Optics Express*. 2020;28(20): 29240. https://doi.org/10.1364/oe.401777

35. Tanaka Y., Murai R., Takahashi Y., … Yoshimura M. Kyropoulos growth of a 300-g SrB_4O_7 single crystal using a twin-type stirring blade. *Japanese Journal of Applied Physics*. 2022;61(7). https://doi.org/10.35848/1347-4065/ac6f35

36. Machida T., Inaba S., Ueda M., Asakawa H., Komatsu R. Growth of transparent SrB_4O_7 crystal fiber by the μ-PD metod. *Transactions of the Materials Research Society of Japan*. 2017;42 (3): 65–68. https://doi.org/10.14723/tmrsj.42.65

37. Jiao Z., Li S., Yan Q., Wang X., Shen D. Growth and optical properties of Eu^{2+}/Li^{+}-co-doped SrB_4O_7 single crystals. *Journal of Physics and Chemistry of Solids*. 2011;72: 252–255. https://doi.org/10.1016/j.jpcs.2011.01.006

38. Evlanova N. F., Naumova I. I., Chaplina T. O., Lavrishchev S. V., Blokhin S. A. Periodic domain structure in Czochralski-grown $LiNbO_3$: Y crystals. *Physics of the Solid State*. 2000;42: 1727–1730. https://doi.org/10.1134/1.1309459

39. Kagebayashi Y., Mori Y., Sasaki T. Crystal growth of cesium triborate, CsB_3O_5 by Kyropoulos technique. *Bulletin of Materials Science*. 1999;22: 971–973. https://doi.org/10.1007/BF02745688

40. Kokh A., Kononova N., Mennerat G., … Kokh K. Growth of high quality large size LBO crystals for high energy second harmonic generation. *Journal of Crystal Growth*. 2010;312: 1774–1778. https://doi.org/10.1016/j.jcrysgro.2010.02.023

41. Armstrong J. A., Bloembergen N., Ducuing J., Pershan P. S. Interactions between light waves in a nonlinear dielectric. *Physical Review. A*. 1962;127: 1918–1939. https://doi.org/10.1103/PhysRev.127.1918

42. Myers L., Miller G., Eckardt R., Fejer M., Byer R., Bosenberg W. Quasi-phase-matched 1.064-μm-pumped optical parametric oscillator in bulk periodically poled $LiNbO_3$. *Optics Letters*. 1995;20: 52–54. https://doi.org/10.1364/OL.20.000052

43. Chen Q., Risk W. Periodic poling of $KTiOPO_4$ using an applied electric field. *Electronics Letters*. 1994;30: 1516–1517. https://doi.org/10.1049/EL:19941019

44. Sonoda S., Tsuruma I., Hatori M. Second harmonic generation in a domain-inverted MgO-doped $LiNbO_3$ waveguide by using a polarization axis inclined substrate. *Applied Physics Letters*. 1997;71: 3048–3050. https://doi.org/10.1063/1.119433

45. Harada M., Muramatsu K.-I., Iwasaki Y., Kurimura S., Taira T. Periodic twinning in crystal quartz for optical quasi-phase matched secondary harmonic conversion. *Journal of Materials Research*. 2004;19(4): 969–972. https://doi.org/10.1557/JMR.2004.0125

46. Ishizuki H., Taira T. Characterization of crystal quartz for QPM wavelength-conversion device. *Optics Express*. 2024;32: 48492. https://doi.org/10.1364/OE.539371

47. Tsuboi Y., Kimura H., Koizumi H., Uda S. Polarization mechanism of $LiNbO_3$ crystal due to thermoelectric power and current-induced electric fields during growth via micro-pulling-down method. *Journal of Crystal Growth*. 2009;311: 4089–4093. https://doi.org/10.1016/j.jcrysgro.2009.06.053

48. Yoon D. H., Yonenaga I., Fukuda T., Ohnishi N. Crystal growth of dislocation-free $LiNbO_3$ single crystals by micro pulling down method. *Journal of Crystal Growth*. 1994;142(3-4): 339–343. https://doi.org/10.1016/0022-0248(94)90342-5

49. Kurlov V. N., Rossolenko S. N., Abrosimov N. V., Lebbou K. Shaped crystal growth. In: *Crystal Growth Processes Based on Capillarity*. T. Duffar (ed.). 2010;5: 277–354. https://doi.org/10.1002/9781444320237.ch5

50. Fukuda T., Rudolph P., Uda S. *Fiber crystal growth from the melt*. Heidelberg: Springer Berlin; 2004. 281 p. https://doi.org/10.1007/978-3-662-07214-1

51. Shi Q., Uda S. Non-steady-state crystal growth of $LiNbO_3$ in the presence of an interface electric field. *Journal of Crystal Growth*. 2021;566–567, 126161. https://doi.org/10.1016/j.jcrysgro.2021.126161

52. Yoshimura M., Mori Y., Hu Z. G., Sasaki T. Growth and characterization of nonlinear optical borate crystals $CsLiB_6O_{10}$, CsB_3O_5, and $BaAlBO_3F_2$. *Optical Materials*. 2004;26(4): 421–423. https://doi.org/10.1016/j.optmat.2003.12.026

53. Nishioka M., Kanoh A., Yoshimura M., Mori Y., Sasaki T. Growth of $CsLiB_6O_{10}$ crystals with high laser-damage tolerance. *Journal of Crystal Growth*. 2005;279: 76–81. https://doi.org/10.1016/j.jcrysgro.2004.11.418

54. Kokh A., Vlezko V., Kokh K., Kononova N., Villeval Ph., Lupinski D. Dynamic control over the heat field during LBO crystal growth by High temperature solution method. *Journal of Crystal Growth*. 2012;360: 158–161. https://doi.org/10.1016/j.jcrysgro.2011.11.050

55. Zhao S., Huang C., Zhang H. Crystal growth and properties of lithium triborate. *Journal of Crystal Growth*. 1990;99: 805–810. https://doi.org/10.1016/S0022-0248(08)80030-9

56. Martynyuk-Lototska I., Mys O., Krupych O., ... Schranz W. Elastic, piezooptic and acoustooptic properties of borate crystals (BaB_2O_4, $Li_2B_4O_7$ and $CsLiB_6O_{10}$). *Integrated Ferroelectrics*. 2004;(1): 99–103. https://doi.org/10.1080/10584580490458801

57. Laugier M. T. New formula for indentation toughness in ceramics. *Journal of Materials Science Letters*. 1987;6: 355–356. https://doi.org/10.1007/BF01729352

58. Bohaty L. Elektrooptische und elektrostriktive eigenschaften von bleitetraborat PbB_4O_7. *Zeitschrift für Kristallographie*. 1983;164: 279–283. https://doi.org/10.1524/ZKRI.1983.164.3-4.279

59. V'yunyshev A. M., Aleksandrovskii A. S., Cherepakhin A. V., Rovskii V. E., Zaitsev A. I., Zamkov A. V. Frequency doubling of ultrashort pulses in a nonlinear photonic strontium tetraborate crystal. *Bulletin of the Lebedev Physics Institute*. 2010;37(3): 85–86. https://doi.org/10.3103/s106833561003005x

60. Trabs P., Noack F., Aleksandrovsky A. S., Zaitsev A. I., Petrov V. N. Generation of coherent radiation in the vacuum ultraviolet using randomly quasi-phase-matched strontium tetraborate. *Optics Letters*. 2016:41(3): 618–621. http://dx.doi.org/10.1364/OL.41.000618

61. Ma Z., Wu K., Sa R., Ding K., Li Q. Strain-induced improvements on linear and nonlinear optical properties of SrB_4O_7 crystal. *AIP Advances*. 2012;2(3): 032170. http://dx.doi.org/10.1063/1.4754277

62. Buryy O., Andruschchak N., Demyanyshyn N., Andruschchak A., Mytsyk B. The acousto-optic effect maxima in SrB_4O_7 crystals. In: *2016 IEEE 13th international conference on laser and fiber-optical networks modeling (LFNM): 13th Int. Conf., 13–15 September 2016*. Odessa, Ukraina: IEEE Publ.; 2016. p. 65–66. https://doi.org/10.1109/LFNM.2016.7851232

63. Buryy O., Andrushak N., Ratych A., Demyanyshyn N., Mytsyk B., Andrushak A. Global maxima for the acousto-optic effect in SrB_4O_7 crystals. *Applied Optics*. 2017;56(7): 1839–1845. https://doi.org/10.1364/AO.56.001839

64. Aleksandrov K. S., Zamkov A. V., Zaitsev A. I., Turchin P. P., Sysoev A. M., Parfenov A. A. Acoustical and acoustooptical properties of lead tetraborate single crystals. *Physics of the Solid State*. 2004:46(9): 1637–1638. https://doi.org/10.1134/1.1799178

65. Martynyuk-Lototska I., Mys O., Dudok T., Adamiv V., Smirnov Y., Vlokh R. Acousto-optic interaction in α-BaB_2O_4 and $Li_2B_4O_7$ crystals. *Applied Optics*. 2008;47(19): 3446–3454. https://doi.org/10.1364/ao.47.003446

66. Mytsyk B., Demyanyshyn N., Martynyuk-Lototska I., Vlokh R. Piezo-optic, photoelastic, and acousto-optic properties of SrB_4O_7 crystals. *Applied Optics*. 2011;50(21): 3889–3895. https://doi.org/10.1364/AO.50.003889

67. Demyanyshyn N. M., Mytsyk B. G., Sakharuk O. M. Elasto-optic effect anisotropy in strontium borate crystals. *Applied Optics*. 2014;53(8): 1620–1628. https://doi.org/10.1364/AO.53.001620

68. Zinenko V. I., Pavlovskii M. S., Zaitzev A. I., Krylov A. S., Shinkorenko A. S. Vibrational spectra and elastic piezoelectric and polarization properties of the α- SrB_4O_7 crystal. *Journal of Experimental and Theoretical Physics*. 2012;115(3): 455–461. https://doi.org/10.1134/S1063776112080195

69. Nambu T., Nagata T., Umeda S., ... Katayama R. Monolithic microcavity second harmonic generation device using low birefringence paraelectric material without polarity-inverted structure. *Applied Physics Express*. 2021;14: 061004. https://doi.org/10.35848/1882-0786/abff9e

70. Nambu T., Yano T., Umeda S., … Katayama R. DUV coherent light emission from ultracompact microcavity wavelength conversion device. *Optics Express*. 2022;30(11): 18628–18637. https://doi.org/10.1364/OE.457538

71. Nambu T., Yoshimura M., Mori Y., … Katayama R. 199 nm vacuum-ultraviolet second harmonic generation from SrB_4O_7 vertical microcavity pumped with picosecond laser. *Applied Physics Express*. 2024;17: 082004. https://doi.org/10.35848/1882-0786/ad69fe

72. Igarashi H., Tamaru Y., Qu C., … Mizoguchi H. Generation of 10w, 1ns deep ultraviolet pulse at 193nm. In: *Conference on lasers and electro-optics europe and european quantum electronics conference: 23–27 June 2019*. Munich Germany: OSA Technical Digest (Optica Publishing Group); 2019. paper ca_4_4. URL: https://opg.optica.org/abstract.cfm?URI=CLEO_Europe-2019-ca_4_4

73. Cherepakhin A. V. *Production, optical and nonlinear optical properties of* α, β-SrB_4O_7 *and* δ-BiB_3O_6. Cand. phys.–math. sci. diss. Krasnoyarsk: 2011. 141 p. URL: https://www.dissercat.com/content/poluchenie-opticheskie-i-nelineino-opticheskie-svoistva-b-srb4o7-i-d-bib3o6

Information about the authors

Tatyana N. Khamaganova, Cand. Sci. (Chem.), Associate Professor, Senior Research Fellow, Laboratory of Oxide Systems, Baikal Institute of Nature Management, Siberian Branch of the Russian Academy of Sciences (Ulan-Ude, Russian Federation).

https://orcid.org/0000-0002-8970-1481
khama@binm.ru

Alexey K. Subanakov, Cand. Sci. (Chem.), Head of the Laboratory of Oxide Systems, Baikal Institute of Nature Management, Siberian Branch of the Russian Academy of Sciences (Ulan-Ude, Russian Federation).

https://orcid.org/0000-0002-1674-283X
subanakov@binm.bscnet.ru

Received September 16, 2025; approved after reviewing November 14, 2025; accepted for publication December 8, 2025; published online September 25, 2026.